Acta Crystallographica Section C
Crystal Structure Communications
ISSN 0108-2701

Nine compounds containing high-nuclearity $[Cu_nX_{2n+2}]^{2-}$ (n = 4, 5 or 7; X = Cl or Br) quasi-planar oligomers

Annette Kelley, Subhash Akkina, Goutham K. Devarapally, Soujanya Nalla, Divya Pasam, Shravani Madhabushi and Marcus R. Bond*

Department of Chemistry, Southeast Missouri State University, Cape Girardeau, MO 63701, USA
Correspondence e-mail: bond@mbond2.st.semo.edu

Received 30 September 2010
Accepted 23 November 2010
Online 18 December 2010

The structures of seven $A_2Cu_4X_{10}$ compounds containing quasi-planar oligomers are reported: bis(1,2,4-trimethylpyridinium) hexa-μ-chlorido-tetrachloridotetracuprate(II), $(C_8H_{12}N)_2[Cu_4Cl_{10}]$, (I), and the hexa-$\mu$-bromido-tetrabromidotetracuprate(II) salts of 1,2,4-trimethylpyridinium, $(C_8H_{12}N)_2[Cu_4Br_{10}]$, (II), 3,4-dimethylpyridinium, $(C_7H_{10}N)_2[Cu_4Br_{10}]$, (III), 2,3-dimethylpyridinium, $(C_7H_{10}N)_2[Cu_4Br_{10}]$, (IV), 1-methylpyridinium, $(C_6H_8N)_2[Cu_4Br_{10}]$, (V), trimethylphenylammonium, $(C_9H_{14}N)_2[Cu_4Br_{10}]$, (VI), and 2,4-dimethylpyridinium, $(C_7H_{10}N)_2[Cu_4Br_{10}]$, (VII). The first four are isomorphous and contain stacks of tetracopper oligomers aggregated through semicoordinate Cu$\cdots X$ bond formation in a $4(\frac{5}{2},\frac{1}{2})$ stacking pattern. The 1-methylpyridinium salt also contains oligomers stacked in a $4(\frac{5}{2},\frac{1}{2})$ pattern, but is isomorphous with the known chloride analog instead. The trimethylphenylammonium salt contains stacks of oligomers arranged in a $4(\frac{3}{2},\frac{1}{2})$ stacking pattern similar to the tetramethylphosphonium analog. These six structures feature inversion-related organic cation pairs and hybrid oligomer/organic cation layers derived from the parent CuX_2 structure. The 2,4-dimethylpyridinium salt is isomorphous with the known (2-amino-4-methylpyridinium)$_2Cu_4Cl_{10}$ structure, in which isolated stacks of organic cations and of oligomers in a $4(\frac{1}{2},\frac{1}{2})$ pattern are found. In bis(3-chloro-1-methylpyridinium) octa-μ-bromido-tetrabromidopentacuprate(II), $(C_6H_7ClN)[Cu_5Br_{12}]$, (VIII), containing the first reported fully halogenated quasi-planar pentacopper oligomer, the oligomers stack in a $5(\frac{3}{2},\frac{1}{2})$ stacking pattern as the highest nuclearity $[Cu_nX_{2n+2}]^{2-}$ oligomer compound known with isolated stacking. Bis(2-chloro-1-methylpyridinium) dodeca-μ-bromido-tetrabromidoheptacuprate(II), $(C_6H_7ClN)_2[Cu_7Br_{16}]$, (IX), contains the second heptacopper oligomer reported and consists of layers of interleaved oligomer stacks with a $7[(\frac{7}{2},\frac{1}{2})][(-\frac{9}{2},-\frac{1}{2})]$ pattern isomorphous with that of the known 1,2-dimethylpyridinium analog. All the oligomers reported here are inversion symmetric.

Comment

Linear $[Cu_nX_{2n+2}]^{2-}$ oligomers (X = Cl or Br) exhibit a wide range of structural variation. Among the simplest are isolated dicopper oligomers formed by edge-sharing CuX_4 flattened tetrahedra. More complicated structures are formed when oligomers aggregate into stacks, in which copper(II) ions from one oligomer form long semicoordinate bonds to halide ions in neighboring oligomers. Here, edge-sharing distorted CuX_4 square planes yield quasi-planar oligomers that stack with a plethora of arrangements (Bond & Willett, 1989). The simplest stacking has translationally equivalent oligomers, but ranges in complexity from there to the five-oligomer repeat sequence observed in (4-methylpyridinium)$_2Cu_3Br_8$ (Bond, Willett & Rubenaker, 1990). To represent oligomer stacking, Geiser, Willett *et al.* (1986) developed simple envelope diagrams and a distinctive notation. A rectangular envelope represents the oligomer, with diagonal lines inside for the *trans* X—Cu—X bonds of the CuX_4 squares, which ideally meet the edges and corners at the ligand positions and intersect at the Cu^{2+} positions. The envelopes are stacked offset so that some, or all, of the Cu^{2+} ions of one oligomer sit above or below the halide ions of the neighbors. The corresponding notation starts with a number denoting the nuclearity of the oligomer. Following this, in parentheses, are length measurements (as fractional multiples of the CuX_4 edge length) that describe how far the neighboring oligomer is offset, first parallel and then perpendicular to the long axis of the oligomer. As many offset measurements are appended as are needed to establish the repeat unit of the stack. If an oligomer is a member of two different interleaved stacks, the pattern for each individual stack is enclosed in square brackets. Weise & Willett (1993) have shown that the various stacking patterns can be derived from the layer structure of $CuCl_2$ or $CuBr_2$ by terminating sections of the layers with additional halide ions (accompanied by counter-ions) and also, for more complicated patterns, including stacking faults. Envelope diagrams and their stacking notations for the structures reported in this paper are presented in Fig. 1.

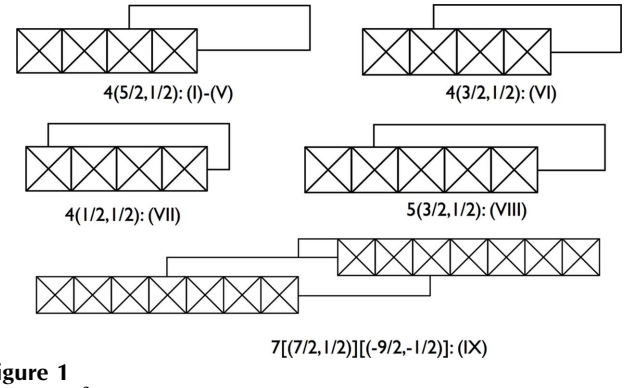

Figure 1
$[Cu_nX_{2n+2}]^{2-}$ quasiplanar oligomer envelope stacking diagrams and their corresponding notation for compounds (I)–(IX).

  doi:10.1107/S0108270110049024

The first, prototypical, oligomer compounds were $LiCuCl_3{\cdot}2H_2O$ (Vossos *et al.*, 1960, 1963), but more particularly $K_2Cu_2Cl_6$ and $(NH_4)_2Cu_2Cl_6$ (Willett *et al.*, 1963), in which H_2O is not semicoordinated to the $Cu_2Cl_6^{2-}$ complex. A survey of the Cambridge Structural Database (CSD, Version 5.31; Allen, 2002) shows approximately 20 such dicopper oligomer compounds have since been discovered, and at least ten similar compounds with neutral N- or O-atom donors for up to two terminal ligands. (Isolated dicopper oligomers, composed of edge-sharing flattened tetrahedra, are present in approximately 40 known compounds.) Oligomer compounds of the form $A_2Cu_3X_8$, with at least ten known examples, are less common, and examples become more rare as the nuclearity increases. Seven $A_2Cu_4X_{10}$ oligomer compounds have been reported to date: $[(CH_3)_3NH]_2Cu_4X_{10}$ [X = Cl (Caputo *et al.*, 1976), CSD refcode MEAMCU10, stacking pattern $4(\frac{3}{2},\frac{1}{2})$; X = Br (Geiser, Willett *et al.*, 1986), CIVNAW10, $4(\frac{3}{2},\frac{1}{2})(\frac{1}{2},-\frac{1}{2})$], (2-amino-4-methylpyridinium)$_2Cu_4Cl_{10}$ [Halvorson *et al.* (1987), FIRWEI, $4(\frac{1}{2},\frac{1}{2})$], $[(CH_3)_4N]_2Cu_4Cl_{10}$ [Halvorson *et al.* (1987), FIRWIM, $4(\frac{3}{2},\frac{1}{2})$], $[(CH_3)_4P]_2Cu_4Br_{10}$ [Murray & Willett (1991), VOGROY, $4(\frac{3}{2},\frac{1}{2})$], (1-methylpyridinium)$_2Cu_4Cl_{10}$ [Bond *et al.* (1995), ZACSEB, $4(\frac{5}{2},\frac{1}{2})$] and (2-chloro-4-methylanilinium)(4-methylanilinium)Cu_4Cl_{10} [Fu & Chivers (2006), GEJTEV, $4(\frac{3}{2},\frac{1}{2})$]. Pentanuclear $Cu_5Cl_{10}(^i PrOH)_2$ [Willett & Rundle (1964), PCUCPR, $5(\frac{3}{2},\frac{1}{2})$; redetermined by Pon & Willett (1996), PCUCPR02] was for many years the highest nuclearity oligomer known. Here, the oligomer stacks are not isolated but are linked to neighboring stacks through semicoordinate bond formation to generate a herringbone pattern, an arrangement also found in GEJTEV. The hexanuclear oligomer compound (1,2-dimethylpyridinium)$_2Cu_6Cl_{14}$ was first reported by Zhou *et al.* (1988) {ZACSIF, $6[(\frac{5}{2},\frac{1}{2})][(-\frac{9}{2},-\frac{1}{2})]$}, with full structural details of this and the related heptanuclear oligomer compound (1,2-dimethylpyridinium)$_2Cu_7Br_{16}$ {ZACSOL, $7[(\frac{7}{2},\frac{1}{2})][(-\frac{9}{2},-\frac{1}{2})]$} provided by Bond *et al.* (1995). These hexa- and heptanuclear compounds contain interdigitated, rather than isolated, stacks of oligomers. A second hexanuclear oligomer compound, $(n\text{-}C_3H_7NH_3)_2Cu_6Cl_{14}$ [Fu & Chivers (2006), GEJTAR, $6(\frac{3}{2},\frac{1}{2})$], obtained through solvothermal synthesis, contains neighboring oligomer stacks in the herringbone arrangement of PCUCPR, rather than the interdigitated stacks of ZACSIF and ZACSOL. The discovery by Haddad *et al.* (2003) of (3,5-dibromopyridinium)$_2Cu_{10}Br_{22}$ {UJODUS, $10[(\frac{7}{2},\frac{1}{2})][(-\frac{15}{2},\frac{1}{2})]$}, containing decacopper oligomers in interdigitated stacks, has dramatically increased known oligomer nuclearity.

During the course of our work on copper(II) halide structural chemistry, we have accumulated several new compounds containing high nuclearity $[Cu_nX_{2n+2}]^{2-}$ oligomers with inversion symmetry. These include seven new compounds containing tetracopper oligomers, namely bis(1,2,4-trimethylpyridinium) hexa-μ-chlorido-tetrachloridotetracuprate(II), (I), and the hexa-μ-bromido-tetrabromidotetracuprate(II) salts of 1,2,4-trimethylpyridinium, (II), 3,4-dimethylpyridinium, (III), 2,3-dimethylpyridinium, (IV), 1-methylpyridinium, (V), trimethylphenylammonium, (VI), and 2,4-dimethylpyridinium, (VII). In addition, we present the second reported examples of a pentanuclear oligomer compound, *viz.* bis(3-chloro-1-methylpyridinium) octa-μ-bromido-tetrabromidopentacuprate(II), (VIII), and a heptanuclear oligomer compound, bis(2-chloro-1-methylpyridinium) dodeca-μ-bromidotetrabromidoheptacuprate(II), (IX).

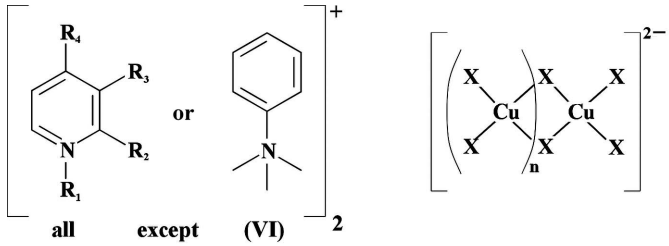

R_1 = CH_3 (I, II, V, VIII, IX)
R_2 = CH_3 (I, II, IV, VII); Cl (IX)
R_3 = CH_3 (III, IV); Cl (VIII)
R_4 = CH_3 (I, II, III, VII)
Otherwise, $R_1 = R_2 = R_3 = R_4 = H$

n = 3 (I-VII); 4 (VIII); 6 (IX)
X = Cl (I), Br (II-IX)

The structures of (I)–(IV) are isomorphous. All crystallize in the monoclinic space group $P2_1/n$ with similar unit-cell constants, and contain translationally equivalent quasi-planar $Cu_4X_{10}^{2-}$ oligomers stacked along a in a $4(\frac{5}{2},\frac{1}{2})$ pattern. Compound (V) is isomorphous with the previously reported chloride analog (ZACSEB) and it bears similarities to, but is not isomorphous with, the structures of (I)–(IV). While (V) does crystallize in the monoclinic space group $P2_1/n$ with an oligomer stacking pattern of $4(\frac{5}{2},\frac{1}{2})$, in this case the translationally equivalent oligomers stack along the monoclinic b axis. The central Cu^{2+} ion (Cu1) is square pyramidal, with four neighboring halide ions within the oligomer forming the basal ligands, while the longer Cu1—X bond to a terminal X5 halide of a neighboring oligomer is apical. The apical ligand induces pyramidalization of the basal ligands, as shown by one *trans* X—Cu1—X angle in the range 161–163° and the other in the range 167–170° for (I)–(IV). The most acute *trans* X—Cu1—X angle is exhibited in (V), which also has the largest difference in *trans* X—Cu1—X angles [158.82 (4) *versus* 170.73 (3)°]. The terminal Cu^{2+} ion (Cu2) is also square pyramidal and forms a longer (~3 Å) semicoordinate bond to the bridging halide X3 of a neighboring oligomer. The more distant apical ligand results in less pyramidalization about Cu2: the X2—Cu2—X5 angle is almost linear (173–175°), while the X3—Cu2—X4 angle (involving the terminal halide ion X4) is more bent (164–168°) for (I)–(V), to give the folded 4+1 coordination environment described previously for ZACSEB. Figs. 2–6

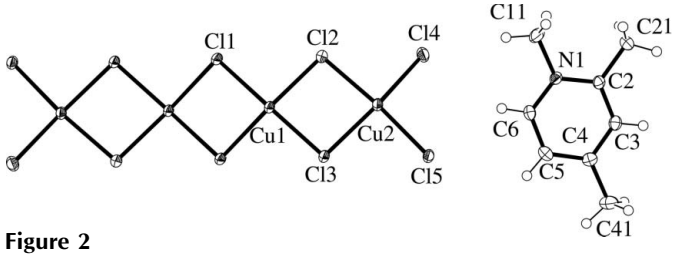

Figure 2
The structure of the organic cation and oligomer of (I), showing the atom-labeling scheme. Displacement ellipsoids are drawn at the 50% probability level.

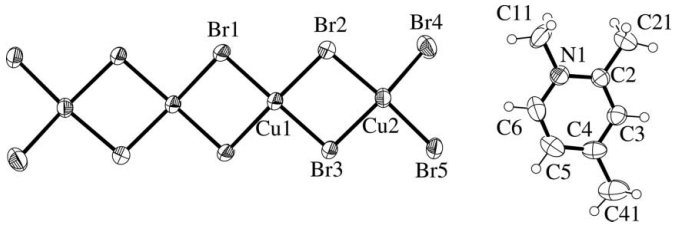

Figure 3
The structure of the organic cation and oligomer of (II), showing the atom-labeling scheme. Displacement ellipsoids are drawn at the 50% probability level.

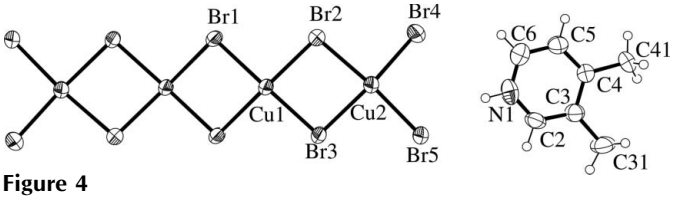

Figure 4
The structure of the organic cation and oligomer of (III), showing the atom-labeling scheme. Displacement ellipsoids are drawn at the 50% probability level.

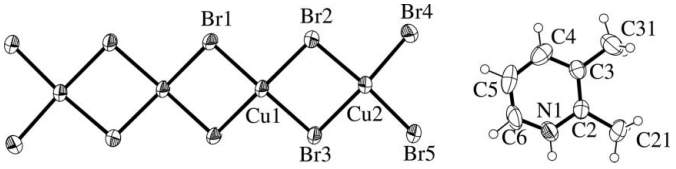

Figure 5
The structure of the organic cation and oligomer of (IV), showing the atom-labeling scheme. Displacement ellipsoids are drawn at the 50% probability level.

present displacement ellipsoid plots of the organic cation and oligomer for compounds (I)–(V), respectively, and Tables 1–3, 5 and 7, respectively, present geometric parameters for these oligomers. Tables 4 and 6 present hydrogen-bond geometries for (III) and (IV), respectively. A packing diagram for (I) is presented in Fig. 7 and is also representative of (II)–(IV).

The oligomer planes are substantially tilted relative to the stacking axis, forming stacking angles of 66.87 (1), 66.54 (1), 70.01 (1), 68.30 (1) and 65.51 (1)° between their mean-plane normals and the stacking axes for (I)–(V), respectively. These values are all lower than the ideal value of 74.499° found for $4(\frac{5}{2},\frac{1}{2})$ stacking with Cu—*X* bonds of the same length and *X*—Cu—*X* and Cu—*X*—Cu angles of 90 or 180°. Longer semi-coordinate bonds between oligomers tend to decrease the stacking angle by further separating the oligomers. On the other hand, outer *X*—Cu—*X* and bridging Cu—*X*—Cu angles greater than 90° [90–94 and 93–95°, respectively, for (I)–(V)] result from lengthening of the oligomer and tend to increase the stacking angle. The stacking angle is also increased by stretching of the oligomer stacks along the stacking axis, as evidenced by outer angles between the basal and apical ligands being greater than the inner angles for square-pyramidal Cu1. Since the stacking angle is smaller than the ideal, semicoordinate bond lengthening is clearly the strongest factor in deviations from it.

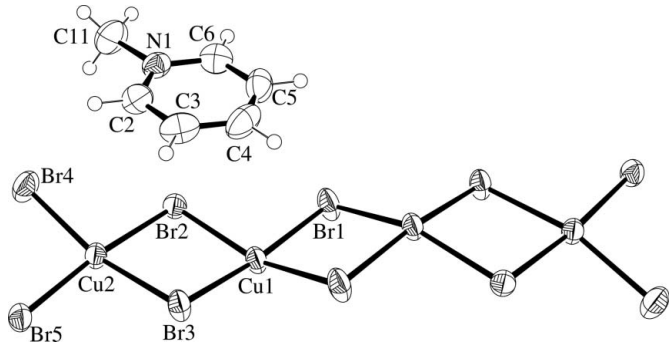

Figure 6
The structure of the organic cation and oligomer of (V), showing the atom-labeling scheme. Displacement ellipsoids are drawn at the 50% probability level.

The organic cations form stacks of inversion-related facing pairs between parallel oligomer stacks. The organic cation planes are almost coplanar with the oligomer planes of a given stack, forming angles of 15.43 (4), 12.20 (7), 8.0 (1), 3.8 (3) and 8.6 (1)° between the normals of the mean oligomer planes for (I)–(V), respectively, and are located at the ends of the oligomers to provide charge compensation for the terminal halides. Each cation of the pair terminates a different oligomer in translationally equivalent stacks, along *b* for (I)–(IV) and along *a* for (V). The organic ring also sits above part of the neighboring oligomer it faces, to block further coordination of Cu^{2+}. This structural feature was first noted in ZACSEB and attributed to the presence of the quaternary 1-methyl-

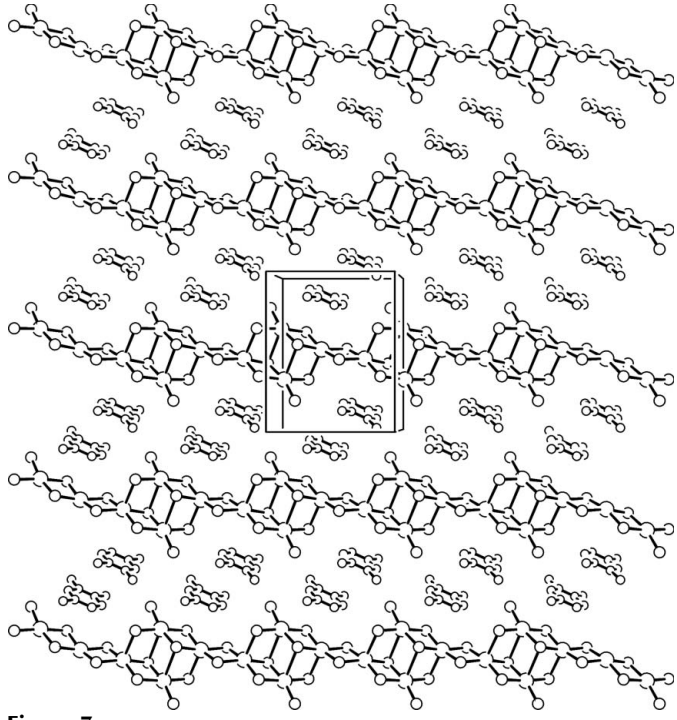

Figure 7
A unit-cell packing diagram for (I), viewed down *c*, with *a* horizontal and *b* vertical, showing the hybrid organic cation/oligomer layer. For clarity, H atoms have been omitted. N and C atoms are drawn as small circles, Cl atoms as medium-sized circles, and Cu atoms as large circles.

pyridinium cation. In the absence of hydrogen bonding, it was thought that optimizing the out-of-plane electrostatic attraction between the quaternary N atom and a halide ion in a facing oligomer would be the dominant factor in this positioning of the organic ring. A short out-of-plane N$\cdots X$ contact distance [N1$\cdots$Cl2^{i} = 3.404 (2) Å in (I), N1$\cdots$Br2^{i} = 3.578 (5) Å in (II) and N1$\cdots$Br2 = 3.575 (4) Å in (V); symmetry code: (i) $x+1, y, z$] is also found for the quaternary pyridinium cation in (I), (II) and (V). However, in (III), where hydrogen bonding is present, a comparable contact [N1$\cdots$Br1^{i} = 3.672 (7) Å] is found as well. The cation in (IV) has its N atom placed above the mid-point between two bridging bromide ions to form two simultaneous, but longer, interactions [N1$\cdots$Br1^{i} = 4.005 (7) Å and N1$\cdots$Br2^{i} = 4.071 (8) Å]. Here, packing of the methyl groups in a similar manner to that found in (III) places the N atom in this bifurcated arrangement and directs the hydrogen bond to an oligomer in a neighboring stack. So the out-of-plane interaction between a pyridinium cation and the planar oligomer can be more generally applied beyond the quaternary pyridinium cation for which it was first noted.

The organic cations also form inversion-related end-to-end pairs with a very small interplanar spacing [0.431 (7), 0.562 (15), 0.850 (20), 0.435 (23) and 0.455 (14) Å for (I)–(V), respectively] that involve cations of neighboring facing pairs. These end-to-end cation pairs abut approximately coplanar oligomers, and *vice versa*, to establish hybrid organic cation/oligomer ribbons through the structure. The ribbons stack to form layers in the *ab* plane, so that the ribbon planes are parallel to (130) or ($\bar{1}$30) in alternating layers [(310) or ($\bar{3}$10) for (V)]. The interplanar spacing between organic cations in the facing pair [3.498 (3), 3.681 (6), 3.612 (8), 3.544 (12) and 3.478 (6) Å for (I)–(V), respectively] is not dramatically longer than the typical Cu—X semicoordinate bond distance. So the facing cation pairs fit easily together with the oligomer stacks to establish a hybrid organic cation/oligomer layer structure in the *ab* plane, reminiscent of the layered CdI_2-type structures of $CuCl_2$ or $CuBr_2$. Such a description has been used for a series of structures, *e.g.* $[(CH_3CH_2)_3NCH_3]Cu_3Cl_7$ (LABXEC), in which holes in the CuX_2 layer structure produced by the absence of a $[Cu_nX_{2n-2}]^{2+}$ fragment are occupied by pairs of organic monocations (Weise & Willett, 1993). The $[(CH_3CH_2)_4N]_2Cu_5Cl_{12}$ structure (ZOKCEH), in particular, features holes produced by the removal of $Cu_4Cl_6^{2+}$ fragments to leave parallel stacks of $Cu_4Cl_{10}^{2-}$ oligomers in a $4(\frac{5}{2},\frac{1}{2})$ pattern, linked to one another by $CuCl_4$ square planes (Ayllón *et al.*, 1996). Removing the linking complexes, now by removing $Cu_5X_8^{2+}$ fragments, leaves isolated stacks of $4(\frac{5}{2},\frac{1}{2})$ oligomers. Placing facing organic cation pairs in these holes would then give the layer structures of (I)–(V). In fact, the smallest fragment removed from the CuX_2 layer that produces isolated $4(\frac{5}{2},\frac{1}{2})$ stacked oligomers is planar $Cu_3X_4^{2+}$, as illustrated in Fig. 8. Holes of arbitrarily large size can be produced by adding an appropriate number of $CuCl_2$ units to this smallest fragment. Thus, the layer structures of (I)–(V) may be considered as either cation pairs occupying holes in the CuX_2 layer left by removal of $Cu_3X_4^{2+}$ fragments with expansion of the layer to accomodate the cations, or as cation pairs occupying holes in the CuX_2 layer produced by removal of larger fragments that match the cation-pair size. Oligomer stacks in neighboring layers are then arranged to be directly adjacent to cation-pair stacks, and *vice versa*.

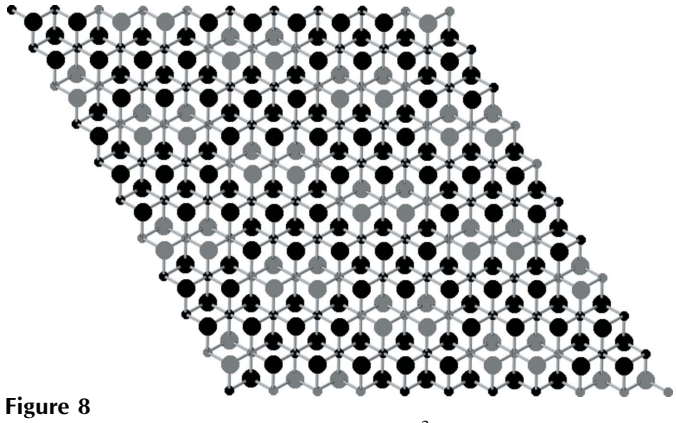

Figure 8
The CuX_2 layer structure, showing the $Cu_3X_4^{2+}$ units, highlighted in gray, that leave behind isolated $4(\frac{5}{2},\frac{1}{2})$ stacks when removed.

The aromatic rings are arranged so that the methyl groups in (III)–(V) are located within the organic cation stack, with the long cation axis approximately parallel to the long oligomer axis. In (I) and (II), however, the long axis of the cation is approximately perpendicular to the long axis of the oligomer it terminates. With methyl groups on opposite sides of the aromatic ring, the organic cation in (I) and (II) is longer than those in (III)–(V). To align the long axis of this cation parallel to the long axis of the oligomer would likely force a longer translation between neighboring oligomers in the stack to produce a $4(\frac{7}{2},\frac{1}{2})$ stacking pattern. This stacking pattern allows only half of the Cu^{2+} ions of the oligomer to form semicoordinate bonds, unlike the $4(\frac{5}{2},\frac{1}{2})$ pattern which allows every Cu^{2+} ion to form one semicoordinate bond. While the $4(\frac{7}{2},\frac{1}{2})$ pattern has yet to be observed, the $4(\frac{5}{2},\frac{1}{2})$ pattern is (to date) the most frequently observed $A_2Cu_4X_{10}$ pattern, accounting for six out of the 14 reported structures. This pattern appears to balance successfully semicoordinate bond formation by the Cu^{2+} ions against close assocation of the planar organic cations with the oligomers.

The structure of the trimethylphenylammonium salt, (VI), consists of both translationally equivalent tetracopper oligomers in a $4(\frac{3}{2},\frac{1}{2})$ pattern and inversion-related facing organic cation pairs stacked parallel to *a*. The central Cu^{2+} ion (Cu1) is 4+1+1′ coordinated, with a semicoordinate bond to the terminal bromide ion Br4 and a longer bond to the bridging bromide ion Br2 of opposite neighboring oligomers. The terminal Cu^{2+} ion (Cu2) is 4+1 coordinated, with a semicoordinate bond to the bridging bromide ion Br1 of a neighboring oligomer. For Cu1, the longer semicoordinate ligand is too distant [3.5416 (7) Å] to influence the coordinate ligand geometry substantially, so both Cu^{2+} ions show significant pyramidalization of the coordinate bromide ions, with *trans* Br—Cu—Br angles in the range 167–173°. A displacement ellipsoid plot of the organic cation and oligomer of (VI) is presented in Fig. 9, with a packing diagram for the structure

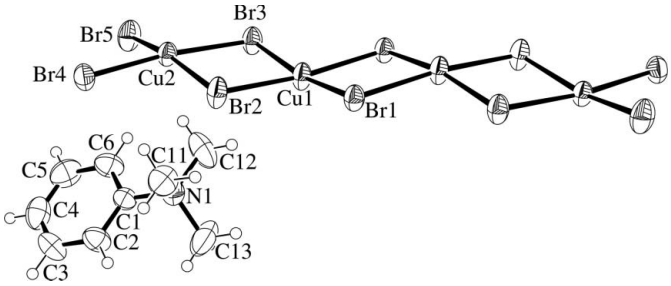

Figure 9
The structure of the organic cation and oligomer of (VI), showing the atom-labeling scheme. Displacement ellipsoids are drawn at the 50% probability level.

presented in Fig. 10. Table 8 lists geometric parameters for the oligomer.

The organic cations and oligomers of (VI) are both tilted relative to *a*, with the long axis of the cation (as defined by the N1···C4 line) forming an angle of 50.96 (9)° and the oligomer plane normal forming an angle of 61.164 (4)° (less than the ideal value of 65.905°) with respect to *a*. The facing pair of organic cations are offset, so that only atom C4 of each ring sits above that of the other ring, with an interplanar spacing between the phenyl rings of 3.376 (7) Å. Each cation is also related by inversion to a cation in a neighboring pair. Here, the two rings are far more offset from one another, with the closest contact of 2.36 Å occurring between H4 atoms. The large offset of these cations precludes any overlap of the phenyl rings and permits a smaller interplanar spacing of 1.471 (11) Å. Organic cation pair stacking is also found in the structure of (trimethylphenylammonium)$_2$Cu$_3$Cl$_8$ (Bond, 2010). In that case, the cation pairs form a longer repeat distance [7.4496 (1) Å, *versus* 6.3969 (1) Å in (VI)] due to closer pairing. Indeed, organic cation repeat distances of 6.1–6.4 Å for (VI), FIRWIM and VOGROY match the repeat distances for other isolated tetramethylammonium cation stacks, for example, in [(CH$_3$)$_4$N]NiX_3 [X = Cl (TMANIC) or Br (TMABNI10); Stucky, 1968]. Thus, the repeat distance in (VI) is consistent with the packing of the trimethylammonium head group. For (trimethylphenylammonium)$_2$Cu$_3$Cl$_8$, the organic cations assume a preferential packing mode which enforces a repeat distance on the chloridocuprate(II) chain that leads to an unusual chain structure. With the larger bromide ion present and a higher ratio of Cu^{2+} to organic cation in (VI), the inorganic portion of the structure now plays a stronger role in defining the packing to produce the more offset cation pairing. The trimethylammonium head group of the cation is directed towards the end of the $Cu_4Br_{10}^{2-}$ oligomer, with the phenyl ring directed away from the oligomer. Similar termination of the oligomer by (CH$_3$)$_4Pn^+$ (*Pn* = N or P) is found for FIRWIM and VOGROY. The interaction between the cation and the oligomer is far less specific here than the out-of-plane interaction that generates the longer $4(\frac{5}{2},\frac{1}{2})$ stacking translation found for compounds (I)–(V). In this case, the intermediate-length parallel translation of the $4(\frac{3}{2},\frac{1}{2})$ pattern could arise simply from the need for the oligomer stacking to match the repeat distance dictated by the

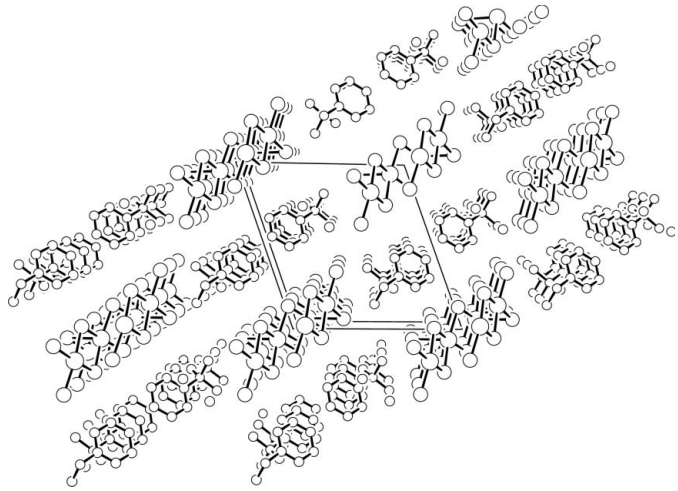

Figure 10
A unit-cell packing diagram for (VI), viewed parallel to *a*, with *b* horizontal and *c* approximately vertical, showing the hybrid organic cation pair/oligomer layers in the $(10\bar{2})$ planes. Oligomer stacks in adjacent layers neighbor cation-pair stacks and *vice versa*. For clarity, H atoms have been omitted. N and C atoms are drawn as small circles, Br atoms as medium-sized circles, and Cu atoms as large circles.

packing of the trimethylammonium head group. Indeed, the structure of the trimethylammonium chloride salt (MEAMCU10) is also isomorphous with FIRWIM, even though the organic cation/oligomer interaction is a specific hydrogen bond that orients the head group away from the oligomer.

The triclinic unit cell of (VI) is not isomorphous with FIRWIM or VOGROY, which crystallize in the monoclinic space group $P2_1/c$. An obvious difference between these structures, then, is that all oligomer stacks in (VI) are translationally equivalent. However, the values for *b* and *c* in (VI) are similar, as are the values for β and γ, which suggests a transformation using the matrix (100, 011, $01\bar{1}$) to a nominal *A*-centered unit cell with (approximately) monoclinic cell constants: a' = 6.3969 (1) Å, b' = 14.2740 (3) Å, c' = 19.4957 (3) Å, α' = 88.025 (2)°, β' = 90.046 (1)° and γ' = 108.418 (1)° [compared with a = 6.425 (2) Å, b = 20.379 (6) Å, c = 11.243 (3) Å and β = 98.52 (2)° for VOGROY]. [The transformed b' axis is significantly longer than the corresponding axis (*c*) in VOGROY because it aligns closely to the long axis of the trimethylphenylammonium cation.] In spite of the geometric similarities between these structures, (VI) is distinctly different. The oligomer stacks and organic cation pairs form layers parallel to $(01\bar{2})$ that are reminiscent of $CuBr_2$ layers. In this case, the layers can be conceived as inserting organic cation pairs into holes formed by removing planar $Cu_2Br_2^{2+}$ fragments (as shown in Fig. 11). Layers are arranged as in (I)–(V) so as to sandwich cation-pair stacks with oligomer stacks and *vice versa*. This layer description is not, however, apparent for the (CH$_3$)$_4Pn^+$ salts, where distinct organic cation pairing is not present and the oligomer stacks are canted with respect to any possible layer plane.

$A_2Cu_4X_{10}$ structures for other variations of the tetramethylammonium cation have not yet been identified. The simplest variation would be ethyltrimethylammonium, for

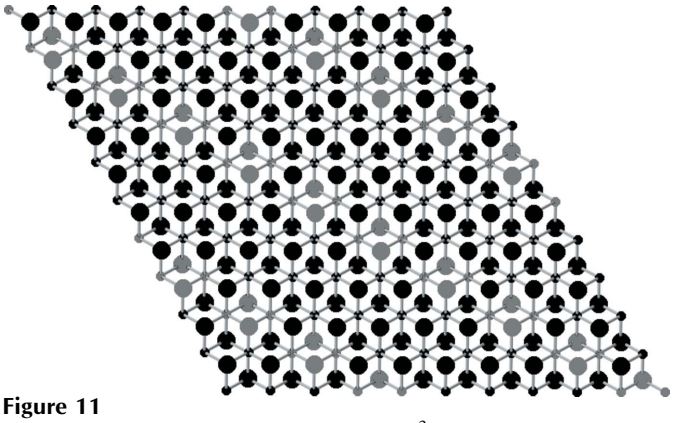

Figure 11
The CuX_2 layer structure, showing the $Cu_2X_2^{2+}$ units, highlighted in gray, that leave behind isolated $4(\frac{3}{2},\frac{1}{2})$ stacks when removed.

which a $[Cu_5Cl_{14}^{4-}]_n$ chain structure is known (Bond, Willett *et al.*, 1990), but it appears that no attempt has been made to prepare $Cu_4X_{10}^{2-}$ salts. Based on the structures of (V), FIRWIM, VOGROY and MEAMCU10, a $4(\frac{3}{2},\frac{1}{2})$ oligomer pattern would be expected for such a salt as well. Oligomer structures are known for more highly substituted tetramethylammonium cations. Both diethyldimethyl- (Willett, 1991) and tetraethylammonium (Willett & Geiser, 1986) form compounds with $Cu_4Cl_{12}^{4-}$ oligomers, and triethylmethylammonium forms a $Cu_3Cl_9^{3-}$ oligomer compound (Willett, 1991). In these structures, the bulkiness of the organic cations, and the higher ratio of organic cations to Cu^{2+} ions, prevents aggregation of the oligomers and they are isolated. Likewise, $[(CH_3)_4P]_2Cu_4Cl_{10}$ (Haije *et al.*, 1986; FAMYIB) and $[(CH_3)_4As]_2Cu_4Cl_{10}$ (Murray & Willett, 1993; LATRON) both occur as complicated layer structures with holes occupied by pairs of organic cations, rather than as stacks of $Cu_4Cl_{10}^{2-}$ oligomers. Thus, organic cation size is a key factor in determining whether quasi-planar oligomers will be formed in this family. In this regard, Geiser, Gaura *et al.* (1986) have invoked the organic cation to halide ion size ratio to account for the difference in stacking patterns between (trimethylammonium)$_2Cu_4Cl_{10}$ and (trimethylammonium)$_2Cu_4Br_{10}$.

The (2,4-dimethylpyridinium)$_2Cu_4Br_{10}$ structure, (VII), is isomorphous with that of (2-amino-4-methylpyridinium)$_2$-Cu_4Cl_{10} (FIRWEI). The unit-cell constants are all larger than for FIRWEI, an obvious result of substituting bromide for chloride. Otherwise the two structures are quite similar. Translationally equivalent organic cations stack parallel to *a*, and are isolated and parallel to translationally equivalent oligomers that stack in a $4(\frac{1}{2},\frac{1}{2})$ pattern. All the Cu^{2+} ions are 4+1+1′ coordinated, with semicoordinate bond lengths greater than 3 Å. Longer semicoordinate bonds lead to weaker distortions from planarity of the coordinate ligands than are observed in (I)–(VI). There is no overlap between the organic ring and the oligomer plane, resulting in the minimum parallel translation of neighboring oligomers within the stack. The oligomer mean plane is less tilted relative to the stacking axis than those in (I)–(VI), the normal forming an angle of 37.842 (6)° with *a*, less than the ideal value of exactly 45°. The organic cations are located at the ends of the oligomers to provide charge compensation for the terminal bromide ions, similar to the arrangements between the organic cations and oligomers found in (I)–(VI). The organic cation is strongly tilted relative to the oligomer in this structure, though, with an angle of 19.4 (2)° between mean plane normals. The hydrogen bonding between the organic cation and the oligomer is much weaker than in (III) and (IV), with H···Br distances approaching 3 Å. Other than providing charge balance in the crystal structure, the organic cations appear to have little interaction with the oligomer. The interplanar spacing between neighboring organic cations in the same stack is 3.751 (7) Å, greater than the sum of the van der Waals radii for two C atoms (Bondi, 1964) and larger than the interplanar spacing between pairs of pyridinium cations in (I)–(V). Thus, there appears to be little or no π–π interaction between neighboring organic cations in the stack. A displacement ellipsoid plot of the organic cation and oligomer of (VII) is presented in Fig. 12, with geometric parameters for the oligomer in Table 9 and hydrogen-bonding parameters in Table 10.

One might first expect (VII) to have a structure similar to that of the closely related pyridinium salts in (I)–(IV). It is also surprising, given the strong effect that hydrogen bonding has been found to have in halidocuprate(II) structures (Geiser, Gaura *et al.* 1986), that replacement of the strongly hydrogen-bonding amino group by a methyl group produces so little structural difference. One similarity between the organic cations in (VII) and FIRWEI is the presence of electron-donating groups, *viz.* –CH_3 and –NH_2, in the *ortho* and *para* positions of the aromatic ring, which, using classical resonance arguments, would both tend to delocalize positive charge away from the N atom. More disperse positive charge would weaken the out-of-plane interaction between the formal charge center of the organic cation and a halide ion in a facing oligomer. Semicoordination to a Cu^{2+} ion of a neighboring oligomer would now be the stronger interaction for the halide ion, thus generating a stacking pattern with the shortest parallel translation and the maximum number of Cu···*X* semi-

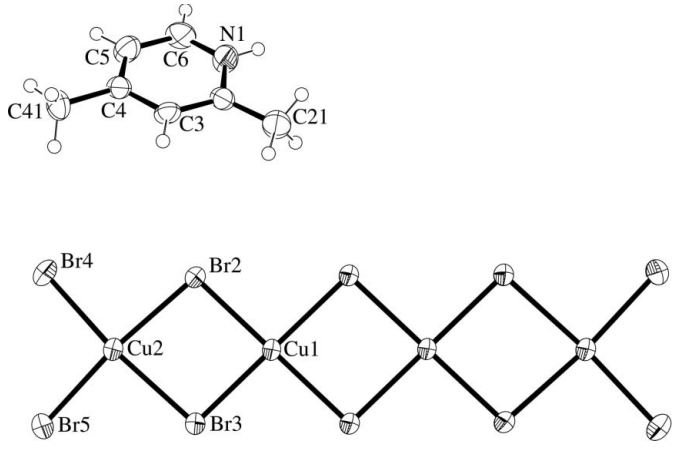

Figure 12
The structure of the organic cation and oligomer of (VII), showing the atom-labeling scheme. Displacement ellipsoids are drawn at the 50% probability level.

coordinate bonds. The direct stacking of the organic cations in (VII), rather than the formation of inversion-related pairs as in (I)–(V), provides some evidence of this charge delocalization, since it places the formal seats of positive charge (N1) in each cation directly above one another in a position that potentially maximizes their repulsion. The 2,3- and 3,4-dimethylpyridinium cations possess only one electron-donating group in the *ortho* or *para* position, presumably resulting in less delocalization of the positive charge and a stronger out-of-plane interaction that results in the $4(\frac{5}{2},\frac{1}{2})$ stacking. Likewise, methylating the ring N atom, as in (II), should counteract delocalization of the positive charge beyond the neighborhood of the ring N atom. The difference in stacking pattern arising from small differences in methyl-group positions on the aromatic cation ring in (II)–(IV) and (VII) illustrates the subtle interplay of forces that often determines a particular pattern.

The (3-chloro-1-methylpyridinium)$_2$Cu$_5$Br$_{12}$ structure, (VIII), contains isolated stacks of translationally equivalent oligomers and of translationally equivalent organic cations parallel to *a*. This is the first reported example of a fully halogenated quasi-planar pentacopper oligomer, and the structure demonstrates that isolated stacking can persist in $[Cu_nX_{2n+2}]^{2-}$ oligomers at least to $n = 5$. The stacking pattern found in (VIII) is $5(\frac{3}{2},\frac{1}{2})$, with the terminal Cu^{2+} atom (Cu3) 4+1 coordinated (the apical bond being to a bridging bromide ion Br1 in a neighboring oligomer), the penultimate Cu^{2+} atom (Cu2) 4+1+1′ coordinated (the shorter axial bond being to the terminal bromide ion Br6 and the longer axial bond to the bridging bromide ion Br2 in opposite neighbors), and the central Cu^{2+} atom (Cu1) 4+2 coordinated (the axial bonds being to the bridging bromide ion Br4 in opposite neighbors). The normal to the mean plane of the oligomer forms an angle of 60.188 (1)° relative to the repeat axis, less than the ideal value of 64.761°. The tilt angle of the organic cation is so steep relative to *a* that the cations might almost as well be described as arranged in head-to-tail lines rather than as stacks. The organic cation is almost coplanar with the oligomer [angle between mean plane normals = 1.83 (4)°], and the oligomer and cation planes are arranged close to (103). The cation ring partially overlaps the oligomer plane, with atom N1 sitting almost directly above the terminal bromide ion Br5 [at a distance of 3.555 (3) Å] to generate the $\frac{3}{2}$ parallel translation of neighboring oligomers. The partial overlap of the ring can be ascribed to the position of the chloro group, which is directed away from and extends beyond the oligomer, presumably so as to minimize chloride–bromide repulsion. The oligomer stacks themselves are canted relative to one another, so that the CuX_2-derived oligomer/cation-pair layer structure is not apparent. This is consistent with the observed trend in previously discussed tetracopper oligomer structures, where inversion-related organic cation pairs correlate to a layer structure whereas stacked translationally equivalent organic cations do not. A displacement ellipsoid plot of the organic cation and oligomer is presented in Fig. 13 and a packing diagram in Fig. 14. Geometric parameters of the oligomer are presented in Table 11.

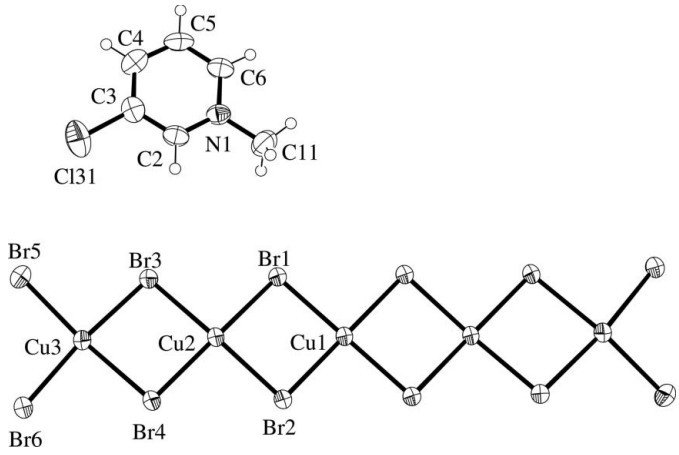

Figure 13
The structure of the organic cation and oligomer of (VIII), showing the atom-labeling scheme. Displacement ellipsoids are drawn at the 50% probability level.

The (2-chloro-1-methylpyridinium)$_2$Cu$_7$Br$_{16}$ structure, (IX), is isomorphous with ZACSOL, the other reported oligomer compound in which the heptacopper oligomers form interleaved stacks with stacking pattern $7[(\frac{7}{2},\frac{1}{2})][(-\frac{9}{2},-\frac{1}{2})]$. The central (Cu1), penultimate (Cu3) and terminal (Cu4) Cu^{2+} ions are 4+2 coordinated, forming semicoordinate bonds to bromide ions (Br7 for Cu1, Br3 and Br5 for Cu3, and Br1 and Br3 for Cu4) in opposite neighbors. The next innermost Cu^{2+} ion (Cu2) is 4+1+1′ coordinated, with the shorter semi-coordinate bond being to the terminal bromide ion Br7 and the longer to the bridging bromide ion Br5 in opposite

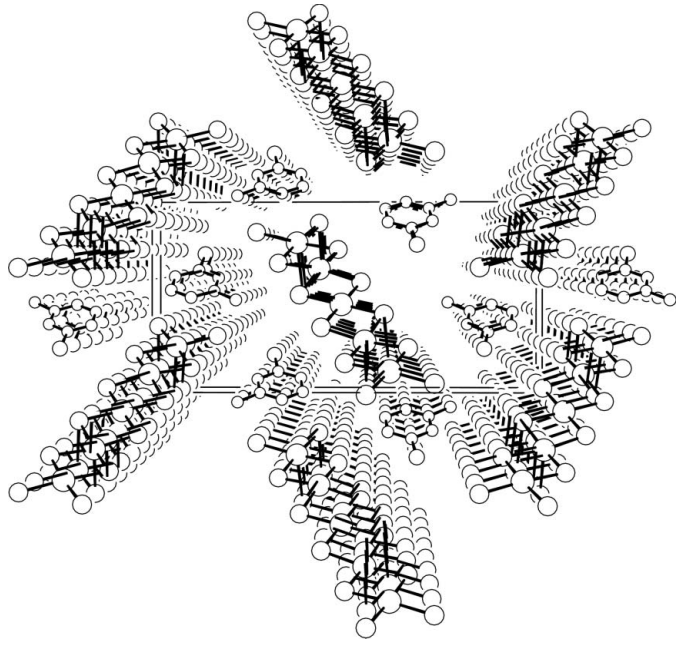

Figure 14
A unit-cell packing diagram for (VIII), viewed parallel to *a* and down the organic cation-pair and oligomer stacks, with *b* horizontal and *c* vertical. For clarity, H atoms have been omitted. N and C atoms drawn as small circles, Cl and Br atoms are drawn as medium size circles, and Cu atoms are drawn as large circles.

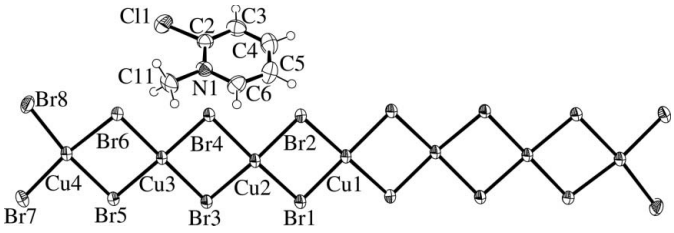

Figure 15
The structure of the major component of the organic cation and oligomer of (IX), showing the atom-labeling scheme. Displacement ellipsoids are drawn at the 50% probability level.

neighbors. A displacement ellipsoid plot of the organic cation and oligomer is presented in Fig. 15, with geometric parameters for the oligomer in Table 12.

The organic cation in ZACSOL, 1,2-dimethylpyridinium, differs from that in (IX) only in an aromatic ring substituent. Hence, the similarity between the structures might be expected, even though the chloro group should interact differently than methyl. It is known that the structures of copper(II) halide compounds can vary dramatically with small changes in organic cation structure, so it is a point of interest that the $[Cu_7Br_{16}^{2-}]_n$ structure remains essentially the same. An analagous situation is found for (4-chloropyridinium)$_2Cu_3Cl_8$ (Zordan *et al.*, 2006; PEGSEA) and (4-methylpyridinium)$_2Cu_3Cl_8$ (Bond, Willett *et al.*, 1990), which also differ chemically in the substitution of chloro for methyl on the aromatic ring. While both contain quasi-planar tricopper oligomers, there are distinct structural differences. PEGSEA is described as being built of mixed cation/anion ribbons, in which the organic cations form bifurcated N—H$\cdots$Cl$_2$Cu hydrogen bonds to the terminal chloride ions at both ends of the oligomer. The organic cations, meanwhile, form symmetric C—Cl$\cdots$Cl—C interactions with one another to form supramolecular dications that complete the ribbon. A similar ribbon motif is found in the methyl analog, although the ribbons are straighter in this case [with a C—C$\cdots$C angle of 170.9 (3)° (Bond & Reynolds, 2010) *versus* a C—Cl$\cdots$Cl angle of 146.9 (2)° in PEGSEA]. This minor difference in the ribbon motif results in major differences between the structures. PEGSEA crystallizes in the triclinic space group $P\overline{1}$, while the methyl analog crystallizes in the monoclinic space group $C2/c$ with significant differences in reduced cell parameters. Also, the oligomer stacking in PEGSEA follows a $3(\frac{1}{2},\frac{1}{2})$ pattern, as opposed to the $3(\frac{1}{2},\frac{1}{2})(\frac{1}{2},-\frac{1}{2})$ pattern found in the methyl analog. In (IX) and ZACSOL, the positions of the substituent groups in the *ortho* positions may restrict the formation of these supramolecular interactions and thus result in very little difference in structure. Furthermore, rather than the ribbon motif found for the *para*-substituted pyridinium structures, the structural motif in the heptacopper oligomer structures is of alternating organic and inorganic layers. The substituent groups of the ring are contained completely within the organic layer, so that the layer structure can likely accomodate small changes in the organic cation without disrupting the bromidocuprate(II) framework.

Experimental

For the quaternary ammonium or pyridinium salts, the tertiary amine, pyridine or substituted pyridine (5 ml) was reacted with excess iodomethane. The resulting iodide salt was converted into the chloride or bromide by halide exchange with excess AgX (X = Cl or Br) in aqueous solution. Otherwise, dimethylpyridine (5 ml) was neutralized with excess concentrated HBr. In all cases, the organic cation halide and copper(II) chloride dihydrate or copper(II) bromide were combined in a 1:2 molar ratio in a solution made 6M in HX. Crystals of (I)–(IX) were obtained upon evaporation.

Compound (I)

Crystal data

$(C_8H_{12}N)_2[Cu_4Cl_{10}]$
M_r = 853.10
Monoclinic, $P2_1/n$
a = 9.0022 (2) Å
b = 11.2121 (4) Å
c = 13.8356 (4) Å
β = 93.016 (2)°
V = 1394.54 (7) Å^3
Z = 2
Mo $K\alpha$ radiation
μ = 3.98 mm^{-1}
T = 100 K
0.20 × 0.09 × 0.06 mm

Data collection

Nonius KappaCCD area-detector diffractometer
Absorption correction: multi-scan (*DENZO*/*SCALEPACK*; Otwinowski & Minor, 1997)
T_{min} = 0.469, T_{max} = 0.793
7229 measured reflections
3736 independent reflections
2991 reflections with $I > 2\sigma(I)$
R_{int} = 0.026

Refinement

$R[F^2 > 2\sigma(F^2)]$ = 0.032
$wR(F^2)$ = 0.077
S = 1.09
3736 reflections
170 parameters
H atoms treated by a mixture of independent and constrained refinement
$\Delta\rho_{max}$ = 0.62 e Å^{-3}
$\Delta\rho_{min}$ = −0.68 e Å^{-3}

Compound (II)

Crystal data

$(C_8H_{12}N)_2[Cu_4Br_{10}]$
M_r = 1297.68
Monoclinic, $P2_1/n$
a = 9.4742 (2) Å
b = 11.7845 (4) Å
c = 14.1290 (4) Å
β = 93.408 (2)°
V = 1574.69 (8) Å^3
Z = 2
Mo $K\alpha$ radiation
μ = 15.36 mm^{-1}
T = 295 K
0.26 × 0.09 × 0.04 mm

Data collection

Nonius KappaCCD area-detector diffractometer
Absorption correction: multi-scan (*DENZO*/*SCALEPACK*; Otwinowski & Minor, 1997)
T_{min} = 0.159, T_{max} = 0.566
7001 measured reflections
3607 independent reflections
2490 reflections with $I > 2\sigma(I)$
R_{int} = 0.040

Refinement

$R[F^2 > 2\sigma(F^2)]$ = 0.039
$wR(F^2)$ = 0.094
S = 1.04
3607 reflections
149 parameters
H-atom parameters constrained
$\Delta\rho_{max}$ = 0.62 e Å^{-3}
$\Delta\rho_{min}$ = −0.55 e Å^{-3}

Table 1
Selected geometric parameters (Å, °) for (I).

Cu1—Cl1	2.2813 (7)	Cu2—Cl2	2.3084 (7)
Cu1—Cl1^{i}	2.2938 (7)	Cu2—Cl3	2.3289 (7)
Cu1—Cl2	2.2840 (7)	Cu2···Cl3^{ii}	2.9485 (8)
Cu1—Cl3	2.2959 (7)	Cu2—Cl4	2.2089 (8)
Cu1···Cl5^{ii}	2.6055 (8)	Cu2—Cl5	2.2620 (7)
Cl1—Cu1—Cl1^{i}	86.48 (3)	Cl2—Cu2—Cl5	173.69 (3)
Cl1—Cu1—Cl2	92.77 (3)	Cl3—Cu2—Cl3^{ii}	86.91 (2)
Cl1^{i}—Cu1—Cl2	163.89 (3)	Cl3—Cu2—Cl4	164.80 (3)
Cl1—Cu1—Cl3	167.89 (3)	Cl3^{ii}—Cu2—Cl4	107.73 (3)
Cl1^{i}—Cu1—Cl3	91.41 (3)	Cl3—Cu2—Cl5	90.76 (3)
Cl1—Cu1—Cl5^{ii}	98.53 (3)	Cl3^{ii}—Cu2—Cl5	85.68 (2)
Cl1^{i}—Cu1—Cl5^{ii}	101.26 (3)	Cl4—Cu2—Cl5	94.32 (3)
Cl2—Cu1—Cl3	85.95 (3)	Cu1—Cl1—Cu1^{i}	93.52 (3)
Cl2—Cu1—Cl5^{ii}	94.78 (3)	Cu1—Cl2—Cu2	94.99 (3)
Cl3—Cu1—Cl5^{ii}	93.58 (2)	Cu1—Cl3—Cu2	94.11 (3)
Cl2—Cu2—Cl3	84.64 (2)	Cu1—Cl3—Cu2^{ii}	85.63 (3)
Cl2—Cu2—Cl3^{ii}	89.76 (2)	Cu2—Cl3—Cu2^{ii}	93.09 (3)
Cl2—Cu2—Cl4	91.21 (3)	Cu1^{ii}—Cl5—Cu2	94.99 (3)

Symmetry codes: (i) $-x, -y, -z+1$; (ii) $-x+1, -y, -z+1$.

Table 2
Selected geometric parameters (Å, °) for (II).

Cu1—Br1	2.4139 (7)	Cu2—Br2	2.4449 (7)
Cu1—Br1^{i}	2.4262 (8)	Cu2—Br3	2.4709 (8)
Cu1—Br2	2.4202 (8)	Cu2···Br3^{ii}	3.1565 (9)
Cu1—Br3	2.4238 (7)	Cu2—Br4	2.3458 (9)
Cu1···Br5^{ii}	2.8042 (9)	Cu2—Br5	2.3915 (7)
Br1—Cu1—Br1^{i}	86.92 (3)	Br2—Cu2—Br5	174.27 (4)
Br1—Cu1—Br2	92.14 (3)	Br3—Cu2—Br3^{ii}	87.02 (2)
Br1^{i}—Cu1—Br2	162.99 (4)	Br3—Cu2—Br4	164.62 (4)
Br1—Cu1—Br3	168.16 (4)	Br3^{ii}—Cu2—Br4	107.58 (3)
Br1^{i}—Cu1—Br3	90.96 (3)	Br3—Cu2—Br5	90.88 (3)
Br2—Cu1—Br3	86.49 (2)	Br3^{ii}—Cu2—Br5	86.94 (2)
Br1—Cu1—Br5^{ii}	97.03 (3)	Br4—Cu2—Br5	94.61 (3)
Br1^{i}—Cu1—Br5^{ii}	101.74 (3)	Cu1—Br1—Cu1^{i}	93.08 (3)
Br2—Cu1—Br5^{ii}	95.24 (3)	Cu1—Br2—Cu2	94.50 (3)
Br3—Cu1—Br5^{ii}	94.81 (3)	Cu1—Br3—Cu2	93.75 (3)
Br2—Cu2—Br3	84.92 (2)	Cu1—Br3—Cu2^{ii}	84.63 (4)
Br2—Cu2—Br3^{ii}	88.93 (2)	Cu2—Br3—Cu2^{ii}	92.98 (4)
Br2—Cu2—Br4	90.43 (3)	Cu1^{ii}—Br5—Cu2	93.52 (3)

Symmetry codes: (i) $-x, -y, -z+1$; (ii) $-x+1, -y, -z+1$.

Table 3
Selected geometric parameters (Å, °) for (III).

Cu1—Br1	2.4152 (10)	Cu2—Br2	2.4376 (10)
Cu1—Br1^{i}	2.4207 (11)	Cu2—Br3	2.4707 (11)
Cu1—Br2	2.4079 (11)	Cu2···Br3^{ii}	3.1049 (12)
Cu1—Br3	2.4321 (9)	Cu2—Br4	2.3540 (11)
Cu1···Br5^{ii}	2.8092 (12)	Cu2—Br5	2.4024 (10)
Br1—Cu1—Br1^{i}	86.95 (3)	Br2—Cu2—Br5	175.19 (4)
Br1—Cu1—Br2	92.12 (4)	Br3—Cu2—Br3^{ii}	88.75 (3)
Br1^{i}—Cu1—Br2	163.25 (5)	Br3—Cu2—Br4	167.67 (5)
Br1—Cu1—Br3	169.69 (5)	Br3—Cu2—Br5	90.20 (3)
Br1^{i}—Cu1—Br3	91.45 (4)	Br3^{ii}—Cu2—Br4	102.81 (4)
Br2—Cu1—Br3	86.48 (3)	Br3^{ii}—Cu2—Br5	86.95 (3)
Br1—Cu1—Br5^{ii}	96.90 (4)	Br4—Cu2—Br5	94.62 (4)
Br1^{i}—Cu1—Br5^{ii}	100.50 (4)	Cu1—Br1—Cu1^{i}	93.05 (3)
Br2—Cu1—Br5^{ii}	96.21 (4)	Cu1—Br2—Cu2	94.51 (4)
Br3—Cu1—Br5^{ii}	93.41 (3)	Cu1—Br3—Cu2	93.07 (3)
Br2—Cu2—Br3	84.99 (3)	Cu1—Br3—Cu2^{ii}	85.98 (30
Br2—Cu2—Br3^{ii}	93.16 (3)	Cu2—Br3—Cu2^{ii}	91.25 (3)
Br2—Cu2—Br4	90.05 (4)	Cu2—Br5—Cu1^{ii}	93.54 (3)

Symmetry codes: (i) $-x, -y, -z+1$; (ii) $-x+1, -y, -z+1$.

Compound (III)

Crystal data

$(C_7H_{10}N)_2[Cu_4Br_{10}]$
M_r = 1269.55
Monoclinic, $P2_1/n$
a = 9.5112 (4) Å
b = 12.3581 (5) Å
c = 12.4617 (6) Å
β = 91.502 (3)°
V = 1464.25 (11) Å^3
Z = 2
Mo $K\alpha$ radiation
μ = 16.52 mm^{-1}
T = 295 K
0.25 × 0.18 × 0.09 mm

Data collection

Nonius KappaCCD area-detector diffractometer
Absorption correction: multi-scan (*DENZO*/*SCALEPACK*; Otwinowski & Minor, 1997)
T_{min} = 0.105, T_{max} = 0.222
6393 measured reflections
3368 independent reflections
2555 reflections with $I > 2\sigma(I)$
R_{int} = 0.032

Refinement

$R[F^2 > 2\sigma(F^2)]$ = 0.046
$wR(F^2)$ = 0.150
S = 1.05
3368 reflections
139 parameters
H-atom parameters constrained
$\Delta\rho_{max}$ = 1.17 e Å^{-3}
$\Delta\rho_{min}$ = −1.46 e Å^{-3}

Compound (IV)

Crystal data

$(C_7H_{10}N)_2[Cu_4Br_{10}]$
M_r = 1269.55
Monoclinic, $P2_1/n$
a = 9.7548 (5) Å
b = 12.5783 (8) Å
c = 12.2179 (5) Å
β = 96.459 (3)°
V = 1489.61 (14) Å^3
Z = 2
Mo $K\alpha$ radiation
μ = 16.24 mm^{-1}
T = 295 K
0.19 × 0.16 × 0.10 mm

Data collection

Nonius KappaCCD area-detector diffractometer
Absorption correction: multi-scan (*DENZO*/*SCALEPACK*; Otwinowski & Minor, 1997)
T_{min} = 0.093, T_{max} = 0.197
7293 measured reflections
3901 independent reflections
2141 reflections with $I > 2\sigma(I)$
R_{int} = 0.074

Refinement

$R[F^2 > 2\sigma(F^2)]$ = 0.050
$wR(F^2)$ = 0.113
S = 1.03
3901 reflections
139 parameters
H-atom parameters constrained
$\Delta\rho_{max}$ = 0.79 e Å^{-3}
$\Delta\rho_{min}$ = −0.93 e Å^{-3}

Compound (V)

Crystal data

$(C_6H_8N)_2[Cu_4Br_{10}]$
M_r = 1241.52
Monoclinic, $P2_1/n$
a = 12.0358 (3) Å
b = 9.5125 (2) Å
c = 12.4133 (3) Å
β = 105.756 (1)°
V = 1367.81 (6) Å^3
Z = 2
Mo $K\alpha$ radiation
μ = 17.68 mm^{-1}
T = 295 K
0.18 × 0.07 × 0.03 mm

Table 4
Hydrogen-bond geometry (Å, °) for (III).

D—H···A	D—H	H···A	D···A	D—H···A
N1—H1···Br5	0.86	2.53	3.364 (7)	163

Table 5
Selected geometric parameters (Å, °) for (IV).

Cu1—Br1	2.4302 (11)	Cu2—Br2	2.4352 (11)
Cu1—Br1^{i}	2.4189 (11)	Cu2—Br3	2.4842 (11)
Cu1—Br2	2.4307 (12)	Cu2···Br3^{ii}	3.1190 (13)
Cu1—Br3	2.4539 (11)	Cu2—Br4	2.3915 (12)
Cu1···Br5^{ii}	2.8266 (14)	Cu2—Br5	2.3870 (11)
Br1^{i}—Cu1—Br1	85.42 (4)	Br2—Cu2—Br3^{ii}	95.83 (4)
Br1—Cu1—Br2	92.68 (4)	Br3—Cu2—Br3^{ii}	92.47 (4)
Br1^{i}—Cu1—Br2	161.13 (6)	Br3—Cu2—Br4	167.24 (5)
Br1—Cu1—Br3	168.34 (6)	Br3—Cu2—Br5	90.15 (4)
Br1^{i}—Cu1—Br3	92.26 (4)	Br4—Cu2—Br5	93.99 (4)
Br2—Cu1—Br3	85.82 (4)	Br3^{ii}—Cu2—Br4	99.84 (4)
Br1—Cu1—Br5^{ii}	99.89 (4)	Br3^{ii}—Cu2—Br5	86.18 (4)
Br1^{i}—Cu1—Br5^{ii}	104.97 (5)	Cu1—Br1—Cu1^{i}	94.58 (4)
Br2—Cu1—Br5^{ii}	93.85 (4)	Cu1—Br2—Cu2	94.74 (4)
Br3—Cu1—Br5^{ii}	91.74 (4)	Cu1—Br3—Cu2	92.94 (4)
Br2—Cu2—Br3	85.06 (4)	Cu1—Br3—Cu2^{ii}	86.80 (4)
Br2—Cu2—Br4	90.32 (4)	Cu2—Br3—Cu2^{ii}	87.53 (4)
Br2—Cu2—Br5	174.87 (5)	Cu2—Br5—Cu1^{ii}	95.13 (4)

Symmetry codes: (i) $-x, -y, -z+1$; (ii) $-x+1, -y, -z+1$.

Table 6
Hydrogen-bond geometry (Å, °) for (IV).

D—H···A	D—H	H···A	D···A	D—H···A
N1—H1···Br4^{iii}	0.86	2.48	3.330 (7)	170

Symmetry code: (iii) $x+\frac{1}{2}, -y+\frac{1}{2}, z-\frac{1}{2}$.

Data collection

Nonius KappaCCD area-detector diffractometer
Absorption correction: multi-scan (*DENZO/SCALEPACK*; Otwinowski & Minor, 1997)
T_{min} = 0.226, T_{max} = 0.618
9228 measured reflections
4736 independent reflections
2706 reflections with $I > 2\sigma(I)$
R_{int} = 0.062

Refinement

$R[F^2 > 2\sigma(F^2)]$ = 0.043
$wR(F^2)$ = 0.091
S = 1.02
4736 reflections
129 parameters
H-atom parameters constrained
$\Delta\rho_{max}$ = 0.89 e Å^{-3}
$\Delta\rho_{min}$ = −0.91 e Å^{-3}

Compound (VI)

Crystal data

$(C_9H_{14}N)_2[Cu_4Br_{10}]$
M_r = 1325.66
Triclinic, $P\overline{1}$
a = 6.3969 (1) Å
b = 11.8734 (2) Å
c = 12.2699 (3) Å
α = 107.693 (1)°
β = 100.607 (1)°
γ = 100.888 (1)°
V = 842.33 (3) Å^3
Z = 1
Mo $K\alpha$ radiation
μ = 14.36 mm^{-1}
T = 295 K
0.21 × 0.17 × 0.14 mm

Data collection

Nonius KappaCCD area-detector diffractometer
Absorption correction: analytical (Alcock, 1974)
T_{min} = 0.104, T_{max} = 0.257
25097 measured reflections
5868 independent reflections
3831 reflections with $I > 2\sigma(I)$
R_{int} = 0.072

Table 7
Selected geometric parameters (Å, °) for (V).

Cu1—Br1	2.4133 (7)	Cu2—Br2	2.4370 (7)
Cu1—Br1^{i}	2.4410 (8)	Cu2—Br3	2.4641 (7)
Cu1—Br2	2.4405 (7)	Cu2···Br3^{ii}	3.1949 (8)
Cu1—Br3	2.4200 (7)	Cu2—Br4	2.3657 (8)
Cu1···Br5^{ii}	2.7658 (8)	Cu2—Br5	2.3792 (7)
Br1—Cu1—Br1^{i}	86.45 (2)	Br2—Cu2—Br5	173.55 (3)
Br1—Cu1—Br2	92.79 (3)	Br3—Cu2—Br3^{ii}	87.09 (2)
Br1^{i}—Cu1—Br2	158.82 (4)	Br3—Cu2—Br4	163.03 (3)
Br1—Cu1—Br3	170.73 (3)	Br3^{ii}—Cu2—Br4	109.56 (3)
Br1^{i}—Cu1—Br3	90.93 (3)	Br3—Cu2—Br5	90.67 (2)
Br2—Cu1—Br3	86.44 (2)	Br3^{ii}—Cu2—Br5	85.05 (2)
Br1—Cu1—Br5^{ii}	94.77 (3)	Br4—Cu2—Br5	93.92 (3)
Br1^{i}—Cu1—Br5^{ii}	105.56 (3)	Cu1—Br1—Cu1^{i}	93.55 (2)
Br2—Cu1—Br5^{ii}	95.60 (3)	Cu1—Br2—Cu2	93.88 (2)
Br3—Cu1—Br5^{ii}	94.49 (2)	Cu1—Br3—Cu2	93.71 (3)
Br2—Cu2—Br3	85.55 (2)	Cu1—Br3—Cu2^{ii}	84.64 (3)
Br2—Cu2—Br3^{ii}	89.54 (2)	Cu2—Br3—Cu2^{ii}	92.91 (3)
Br2—Cu2—Br4	91.19 (3)	Cu2—Br5—Cu1^{ii}	95.71 (2)

Symmetry codes: (i) $-x+1, -y, -z+2$; (ii) $-x+1, -y+1, -z+2$.

Table 8
Selected geometric parameters (Å, °) for (VI).

Cu1—Br1	2.4441 (6)	Cu2···Br1^{ii}	3.0465 (6)
Cu1—Br1^{i}	2.4366 (5)	Cu2—Br2	2.4599 (6)
Cu1—Br2	2.4007 (5)	Cu2—Br3	2.4395 (5)
Cu1···Br2^{ii}	3.5416 (7)	Cu2—Br4	2.4027 (5)
Cu1—Br3	2.4057 (6)	Cu2—Br5	2.3539 (6)
Cu1···Br4^{iii}	2.8987 (7)		
Br1—Cu1—Br1^{i}	87.103 (18)	Br1^{ii}—Cu2—Br4	89.879 (19)
Br1—Cu1—Br2	91.994 (19)	Br1^{ii}—Cu2—Br5	99.19 (2)
Br1^{i}—Cu1—Br2	173.18 (3)	Br2—Cu2—Br3	84.737 (18)
Br1—Cu1—Br2^{ii}	81.905 (18)	Br2—Cu2—Br4	89.557 (19)
Br1^{i}—Cu1—Br2^{ii}	87.475 (18)	Br2—Cu2—Br5	167.34 (3)
Br1—Cu1—Br3	169.07 (3)	Br3—Cu2—Br4	173.23 (2)
Br1^{i}—Cu1—Br3	92.830 (19)	Br3—Cu2—Br5	90.52 (2)
Br1—Cu1—Br4^{iii}	95.24 (2)	Br4—Cu2—Br5	94.31 (2)
Br1^{i}—Cu1—Br4^{iii}	92.774 (19)	Cu1^{i}—Br1—Cu1	92.897 (18)
Br2—Cu1—Br2^{ii}	85.703 (19)	Cu1—Br1—Cu2^{ii}	98.748 (19)
Br2—Cu1—Br3	86.776 (18)	Cu1^{i}—Br1—Cu2^{ii}	86.512 (19)
Br2^{ii}—Cu1—Br3	87.172 (19)	Cu1—Br2—Cu2	94.041 (19)
Br2—Cu1—Br4^{iii}	94.04 (2)	Cu1—Br2—Cu1^{ii}	94.298 (19)
Br2^{ii}—Cu1—Br4^{iii}	177.122 (19)	Cu1^{ii}—Br2—Cu2	86.470 (19)
Br3—Cu1—Br4^{iii}	95.68 (2)	Cu1—Br3—Cu2	94.439 (19)
Br1^{ii}—Cu2—Br2	92.86 (2)	Cu1^{iv}—Br4—Cu2	90.574 (19)
Br1^{ii}—Cu2—Br3	94.023 (19)		

Symmetry codes: (i) $-x+2, -y, -z$; (ii) $-x+1, -y, -z$; (iii) $x+1, y, z$; (iv) $x-1, y, z$.

Refinement

$R[F^2 > 2\sigma(F^2)]$ = 0.045
$wR(F^2)$ = 0.113
S = 1.05
5868 reflections
158 parameters
H-atom parameters constrained
$\Delta\rho_{max}$ = 1.03 e Å^{-3}
$\Delta\rho_{min}$ = −1.26 e Å^{-3}

Compound (VII)

Crystal data

$(C_7H_{10}N)_2[Cu_4Br_{10}]$
M_r = 1269.55
Monoclinic, $P2_1/n$
a = 4.0370 (1) Å
b = 22.3375 (6) Å
c = 15.8508 (3) Å
β = 96.095 (2)°
V = 1421.29 (6) Å^3
Z = 2
Mo $K\alpha$ radiation
μ = 17.02 mm^{-1}
T = 295 K
0.24 × 0.18 × 0.08 mm

Table 9
Selected geometric parameters (Å, °) for (VII).

Cu1—Br1	2.4271 (9)	Cu2—Br2	2.4696 (10)
Cu1—Br1^{i}	2.4237 (9)	Cu2···Br2^{ii}	3.2937 (11)
Cu1···Br1^{ii}	3.2109 (10)	Cu2—Br3	2.5071 (10)
Cu1—Br2	2.3922 (9)	Cu2—Br4	2.3698 (10)
Cu1—Br3	2.4080 (9)	Cu2—Br5	2.3700 (10)
Cu1···Br3^{iii}	3.1074 (10)	Cu2···Br5^{iii}	3.0913 (12)
Br1—Cu1—Br1^{i}	87.24 (3)	Br2—Cu2—Br5	172.50 (4)
Br1^{i}—Cu1—Br1^{ii}	88.39 (3)	Br2^{ii}—Cu2—Br5	87.24 (3)
Br1—Cu1—Br1^{ii}	90.36 (3)	Br2^{ii}—Cu2—Br5^{iii}	175.28 (3)
Br1—Cu1—Br2	92.67 (3)	Br2—Cu2—Br5^{iii}	90.22 (3)
Br1^{i}—Cu1—Br2	178.88 (4)	Br3—Cu2—Br4	169.74 (4)
Br1^{ii}—Cu1—Br2	90.50 (3)	Br3—Cu2—Br5	90.38 (3)
Br1—Cu1—Br3	177.53 (4)	Br3—Cu2—Br5^{iii}	92.09 (3)
Br1^{i}—Cu1—Br3	92.68 (3)	Br4—Cu2—Br5	94.60 (3)
Br1—Cu1—Br3^{iii}	89.24 (3)	Br4—Cu2—Br5^{iii}	96.46 (3)
Br1^{i}—Cu1—Br3^{iii}	91.59 (3)	Br5—Cu2—Br5^{iii}	94.40 (3)
Br1^{ii}—Cu1—Br3	87.17 (3)	Cu1—Br1—Cu1^{i}	92.76 (3)
Br1^{ii}—Cu1—Br3^{iii}	179.60 (3)	Cu1—Br1—Cu1^{iii}	90.36 (3)
Br2—Cu1—Br3	87.36 (3)	Cu1^{i}—Br1—Cu1^{iii}	91.62 (3)
Br2—Cu1—Br3^{iii}	89.53 (3)	Cu1—Br2—Cu2	95.07 (3)
Br3—Cu1—Br3^{iii}	93.23 (3)	Cu1—Br2—Cu2^{iii}	92.32 (3)
Br2—Cu2—Br2^{ii}	87.71 (3)	Cu2—Br2—Cu2^{iii}	87.71 (3)
Br2—Cu2—Br3	83.54 (3)	Cu1—Br3—Cu2	93.71 (3)
Br2^{ii}—Cu2—Br3	83.47 (3)	Cu1—Br3—Cu1^{ii}	93.23 (3)
Br2—Cu2—Br4	90.73 (3)	Cu1^{ii}—Br3—Cu2	94.67 (3)
Br2^{ii}—Cu2—Br4	87.81 (3)	Cu2—Br5—Cu2^{ii}	94.40 (3)

Symmetry codes: (i) $-x+2, -y+1, -z+1$; (ii) $x-1, y, z$; (iii) $x+1, y, z$.

Table 10
Hydrogen-bond geometry (Å, °) for (VII).

D—H···A	D—H	H···A	D···A	D—H···A
N1—H1···Br4^{iv}	0.86	2.84	3.378 (6)	122
N1—H1···Br5^{v}	0.86	3.01	3.573 (6)	125

Symmetry codes: (iv) $x+\frac{1}{2}, -y+\frac{1}{2}, z+\frac{1}{2}$; (v) $x+\frac{3}{2}, -y+\frac{1}{2}, z+\frac{1}{2}$.

Table 11
Selected geometric parameters (Å, °) for (VIII).

Cu1—Br1	2.4106 (3)	Cu2—Br4	2.4095 (5)
Cu1—Br2	2.4096 (3)	Cu2···Br6^{ii}	2.8495 (6)
Cu1···Br4^{i}	3.2587 (4)	Cu3···Br1^{iii}	3.1042 (5)
Cu2—Br1	2.4299 (5)	Cu3—Br3	2.4430 (5)
Cu2—Br2	2.4408 (5)	Cu3—Br4	2.4795 (5)
Cu2···Br2^{i}	3.3991 (5)	Cu3—Br5	2.3724 (5)
Cu2—Br3	2.4199 (5)	Cu3—Br6	2.3867 (5)
Br1—Cu1—Br2	87.770 (10)	Br1^{iii}—Cu3—Br5	97.397 (17)
Br1—Cu1—Br4^{i}	91.784 (10)	Br1^{iii}—Cu3—Br6	88.609 (15)
Br2—Cu1—Br4^{i}	88.629 (9)	Br3—Cu3—Br4	84.716 (15)
Br1—Cu2—Br6^{ii}	93.929 (16)	Br3—Cu3—Br5	91.341 (18)
Br1—Cu2—Br2	86.631 (15)	Br3—Cu3—Br6	173.40 (2)
Br1—Cu2—Br2^{i}	85.665 (15)	Br4—Cu3—Br5	171.27 (2)
Br1—Cu2—Br3	92.161 (17)	Br4—Cu3—Br6	88.791 (17)
Br1—Cu2—Br4	171.06 (2)	Br5—Cu3—Br6	94.927 (17)
Br2—Cu2—Br2^{i}	83.269 (15)	Cu1—Br1—Cu2	92.656 (14)
Br2—Cu2—Br3	169.39 (2)	Cu1—Br1—Cu3^{ii}	93.052 (14)
Br2^{i}—Cu2—Br3	86.130 (16)	Cu2—Br1—Cu3^{ii}	85.212 (14)
Br2—Cu2—Br4	92.806 (17)	Cu1—Br2—Cu2	92.409 (14)
Br2^{i}—Cu2—Br4	85.412 (15)	Cu1—Br2—Cu2^{i}	91.238 (14)
Br2—Cu2—Br6^{ii}	94.928 (17)	Cu2—Br2—Cu2^{i}	96.732 (14)
Br2^{i}—Cu2—Br6^{ii}	178.170 (16)	Cu2—Br3—Cu3	94.582 (17)
Br3—Cu2—Br4	86.751 (16)	Cu2—Br4—Cu3	93.913 (17)
Br3—Cu2—Br6^{ii}	95.671 (18)	Cu1^{i}—Br4—Cu2	94.712 (17)
Br4—Cu2—Br6^{ii}	95.005 (17)	Cu1^{i}—Br4—Cu3	88.146 (17)
Br1^{iii}—Cu3—Br3	92.651 (16)	Cu2^{iii}—Br6—Cu3	91.962 (16)
Br1^{iii}—Cu3—Br4	90.582 (15)		

Symmetry codes: (i) $-x+1, -y, -z$; (ii) $x+1, y, z$; (iii) $x-1, y, z$.

Data collection

Nonius KappaCCD area-detector diffractometer
Absorption correction: multi-scan (*DENZO*/*SCALEPACK*; Otwinowski & Minor, 1997)
T_{min} = 0.111, T_{max} = 0.258

5670 measured reflections
2881 independent reflections
2224 reflections with $I > 2\sigma(I)$
R_{int} = 0.029

Refinement

$R[F^2 > 2\sigma(F^2)]$ = 0.045
$wR(F^2)$ = 0.138
S = 1.07
2881 reflections
137 parameters
H-atom parameters constrained
$\Delta\rho_{max}$ = 1.62 e Å^{-3}
$\Delta\rho_{min}$ = −1.42 e Å^{-3}

Compound (VIII)

Crystal data

$(C_6ClH_7N)[Cu_5Br_{12}]$
M_r = 1533.74
Monoclinic, $P2_1/n$
a = 6.3630 (1) Å
b = 22.9814 (2) Å
c = 11.2713 (1) Å
β = 91.205 (1)°
V = 1647.84 (3) Å^3
Z = 2
Mo $K\alpha$ radiation
μ = 17.90 mm^{-1}
T = 295 K
0.31 × 0.10 × 0.05 mm

Data collection

Nonius KappaCCD area-detector diffractometer
Absorption correction: multi-scan (*DENZO*/*SCALEPACK*; Otwinowski & Minor, 1997)
T_{min} = 0.029, T_{max} = 0.269

14150 measured reflections
7180 independent reflections
5015 reflections with $I > 2\sigma(I)$
R_{int} = 0.035

Refinement

$R[F^2 > 2\sigma(F^2)]$ = 0.038
$wR(F^2)$ = 0.095
S = 1.03
7180 reflections
153 parameters
H-atom parameters constrained
$\Delta\rho_{max}$ = 1.01 e Å^{-3}
$\Delta\rho_{min}$ = −1.02 e Å^{-3}

Compound (IX)

Crystal data

$(C_6H_7ClN)_2[Cu_7Br_{16}]$
M_r = 1980.49
Triclinic, $P\overline{1}$
a = 7.2353 (1) Å
b = 10.7361 (2) Å
c = 12.8913 (2) Å
α = 90.985 (1)°
β = 105.006 (1)°
γ = 100.374 (1)°
V = 949.27 (3) Å^3
Z = 1
Mo $K\alpha$ radiation
μ = 20.84 mm^{-1}
T = 295 K
0.28 × 0.12 × 0.08 mm

Data collection

Nonius KappaCCD area-detector diffractometer
Absorption correction: multi-scan (*DENZO*/*SCALEPACK*; Otwinowski & Minor, 1997)
T_{min} = 0.045, T_{max} = 0.165

9850 measured reflections
5540 independent reflections
3851 reflections with $I > 2\sigma(I)$
R_{int} = 0.030

Refinement

$R[F^2 > 2\sigma(F^2)]$ = 0.038
$wR(F^2)$ = 0.096
S = 1.00
5540 reflections
188 parameters
4 restraints
H-atom parameters constrained
$\Delta\rho_{max}$ = 1.24 e Å^{-3}
$\Delta\rho_{min}$ = −1.01 e Å^{-3}

Table 12
Selected geometric parameters (Å, °) for (IX).

Cu1—Br1	2.4390 (4)	Cu3—Br4	2.4083 (6)
Cu1—Br2	2.4046 (4)	Cu3—Br5	2.4147 (6)
Cu1···Br7^{i}	3.1762 (4)	Cu3···Br5^{ii}	3.1355 (7)
Cu2—Br1	2.4323 (6)	Cu3—Br6	2.3942 (6)
Cu2—Br2	2.4145 (6)	Cu4···Br1^{i}	3.2441 (7)
Cu2—Br3	2.4568 (6)	Cu4···Br3^{ii}	3.2070 (7)
Cu2—Br4	2.4427 (6)	Cu4—Br5	2.4835 (6)
Cu2···Br5^{i}	3.4929 (7)	Cu4—Br6	2.4581 (6)
Cu2—Br7^{ii}	2.7869 (7)	Cu4—Br7	2.3908 (6)
Cu3—Br3	2.4277 (6)	Cu4—Br8	2.3589 (7)
Cu3···Br3^{i}	3.2200 (7)		
Br1—Cu1—Br2	86.919 (13)	Br5^{ii}—Cu3—Br6	89.91 (2)
Br1—Cu1—Br7^{i}	88.407 (13)	Br1^{i}—Cu4—Br3^{ii}	170.38 (2)
Br2—Cu1—Br7^{i}	96.163 (14)	Br1^{i}—Cu4—Br5	88.334 (19)
Br1—Cu2—Br2	86.850 (19)	Br1^{i}—Cu4—Br6	98.05 (2)
Br1—Cu2—Br3	93.44 (2)	Br1^{i}—Cu4—Br7	87.657 (19)
Br1—Cu2—Br4	166.59 (3)	Br1^{i}—Cu4—Br8	87.61 (2)
Br1—Cu2—Br5^{i}	83.61 (2)	Br3^{ii}—Cu4—Br5	86.689 (19)
Br1—Cu2—Br7^{ii}	95.03 (2)	Br3^{ii}—Cu4—Br6	89.59 (2)
Br2—Cu2—Br3	167.62 (3)	Br3^{ii}—Cu4—Br7	84.080 (19)
Br2—Cu2—Br4	90.69 (2)	Br3^{ii}—Cu4—Br8	98.34 (2)
Br2—Cu2—Br5^{i}	88.44 (2)	Br5—Cu4—Br6	83.839 (19)
Br2—Cu2—Br7^{ii}	99.73 (2)	Br5—Cu4—Br7	89.55 (2)
Br3—Cu2—Br4	86.168 (19)	Br5—Cu4—Br8	171.60 (3)
Br3—Cu2—Br5^{i}	79.299 (19)	Br6—Cu4—Br7	171.11 (3)
Br3—Cu2—Br7^{ii}	92.58 (2)	Br6—Cu4—Br8	89.45 (2)
Br4—Cu2—Br5^{i}	83.15 (2)	Br7—Cu4—Br8	97.63 (2)
Br4—Cu2—Br7^{ii}	98.38 (2)	Cu1—Br1—Cu2	92.459 (18)
Br5^{i}—Cu2—Br7^{ii}	171.65 (2)	Cu1—Br1—Cu4^{i}	90.69 (2)
Br3—Cu3—Br3^{i}	88.89 (2)	Cu2—Br1—Cu4^{i}	97.54 (2)
Br3—Cu3—Br4	87.581 (19)	Cu1—Br2—Cu2	93.763 (18)
Br3^{i}—Cu3—Br4	91.64 (2)	Cu2—Br3—Cu3	92.02 (2)
Br3—Cu3—Br5	93.67 (2)	Cu2—Br3—Cu3^{i}	100.58 (2)
Br3—Cu3—Br5^{ii}	89.28 (2)	Cu2—Br3—Cu4^{ii}	85.88 (2)
Br3^{i}—Cu3—Br5	85.760 (19)	Cu3—Br3—Cu3^{i}	91.11 (2)
Br3^{i}—Cu3—Br5^{ii}	172.82 (2)	Cu3—Br3—Cu4^{ii}	91.69 (2)
Br3—Cu3—Br6	179.09 (3)	Cu2—Br4—Cu3	92.84 (2)
Br3^{i}—Cu3—Br6	91.97 (2)	Cu2^{i}—Br5—Cu3	94.34 (2)
Br4—Cu3—Br5	177.09 (3)	Cu2^{i}—Br5—Cu4	90.47 (2)
Br4—Cu3—Br5^{ii}	95.22 (2)	Cu3—Br5—Cu4	94.08 (2)
Br4—Cu3—Br6	92.08 (2)	Cu3—Br6—Cu4	95.26 (2)
Br5—Cu3—Br5^{ii}	87.43 (2)	Cu1^{i}—Br7—Cu4	93.24 (2)
Br5—Cu3—Br6	86.71 (2)	Cu2^{ii}—Br7—Cu4	97.36 (2)

Symmetry codes: (i) $-x+1, -y+2, -z$; (ii) $-x+2, -y+2, -z$.

With the exception of (I) and (IX) (see below), all H-atom positions were calculated using a riding model, with aromatic C—H = 0.93 Å, methyl C—H = 0.96 Å and aromatic N—H = 0.86 Å, and with U_{iso}(H) = 1.2U_{eq}(C,N) for aromatic ring H atoms or 1.5U_{eq}(C) for methyl H atoms. Bond lengths and angles within the organic cations conform to expected values (Ladd & Palmer, 1994). Secondary extinction corrections were refined (Alcock, 1974).

For (I), aromatic H-atom positions and isotropic displacement parameters were refined [C—H = 0.89 (4)–0.91 (4) Å], while methyl H atoms were fixed in a riding model (C—H = 0.96 Å) with refined isotropic displacement parameters.

For (IX), the initial refinement of an ordered model yielded a 2-chloro-1-methylpyridinium cation with anomalously large displacement parameters for atoms N1 and Cl2, anomalously small displacement parameters for atoms C2 and C11, an anomalously short C2—Cl2 bond length and an anomalously long N1—C11 bond length. This suggested static disorder of the organic cation in which the cation is occasionally flipped so that atoms N1 and C2, and C11 and Cl2, change places. A disordered model was refined in which the minor component atoms N1*A* and C2*A* were required to occupy the same positions with the same displacement parameters as C2 and N1, respectively, and the N—CH_3 and C—Cl bond lengths were tightly restrained to 1.4700 (1) and 1.7600 (1) Å, respectively. Anisotropic displacement parameters were refined for the non-H atoms of the ring, but only for the major disorder component of the subsitutents (C11 and Cl2). H-atom positions were calculated using a riding model as described above, except for the minor component of C11 for which no H-atom postions were included. The site occupancy of the major component refined to 0.834 (4). Low angle reflections obscured by the beam catcher shadow, as indicated by $F_o << F_c$, were omitted from the refinement in structures (I), (II), (IV), (V), (VII) and (VIII).

For all compounds, data collection: *COLLECT* (Nonius, 1998); cell refinement: *SCALEPACK* (Otwinowski & Minor, 1997); data reduction: *DENZO* and *SCALEPACK* (Otwinowski & Minor, 1997); program(s) used to solve structure: *SIR92* (Altomare *et al.*, 1993); program(s) used to refine structure: *SHELXL97* (Sheldrick, 2008); molecular graphics: *ORTEP-3 for Windows* (Farrugia, 1997) and *ORTEPIII* (Burnett & Johnson, 1996); software used to prepare material for publication: *WinGX* (Farrugia, 1999).

The authors thank the National Science Foundation DUE CCLI–A&I program (grant No. 9951348) and Southeast Missouri State University for funding the X-ray diffraction facility.

Supplementary data for this paper are available from the IUCr electronic archives (Reference: SK3391). Services for accessing these data are described at the back of the journal.

References

Alcock, N. W. (1974). *Acta Cryst.* A**30**, 332–335.
Allen, F. H. (2002). *Acta Cryst.* B**58**, 380–388.
Altomare, A., Cascarano, G., Giacovazzo, C. & Guagliardi, A. (1993). *J. Appl. Cryst.* **26**, 343–350.
Ayllón, J. A., Santos, I. C., Henriques, R. T., Almeida, M., Alcácer, L. & Duarte, M. T. (1996). *Inorg. Chem.* **35**, 168–172.
Bond, M. R. (2010). *Acta Cryst.* C**66**, m17–m21.
Bond, M. R., Place, H., Wang, Z., Willett, R. D., Liu, Y., Grigereit, T. E., Drumheller, J. E. & Tuthill, G. F. (1995). *Inorg. Chem.* **34**, 3134–3141.
Bond, M. R. & Reynolds, B. J. (2010). Unpublished work.
Bond, M. R. & Willett, R. D. (1989). *Inorg. Chem.* **28**, 3267–3269.
Bond, M. R., Willett, R. D. & Rubenaker, G. V. (1990). *Inorg. Chem.* **29**, 2713–2720.
Bond, M. R., Willett, R. D., Rubins, R. S., Zhou, P., Zaspel, C. E., Hutton, S. L. & Drumheller, J. E. (1990). *Phys. Rev. B*, **42**, 10280–10290.
Bondi, A. (1964). *J. Phys. Chem.* **68**, 441–451.
Burnett, M. N. & Johnson, C. K. (1996). *ORTEPIII*. Report ORNL-6895. Oak Ridge National Laboratory, Tennessee, USA.
Caputo, R. E., Vukosavovich, M. J. & Willett, R. D. (1976). *Acta Cryst.* B**32**, 2516–2518.
Farrugia, L. J. (1997). *J. Appl. Cryst.* **30**, 565.
Farrugia, L. J. (1999). *J. Appl. Cryst.* **32**, 837–838.
Fu, Z. & Chivers, T. (2006). *Can. J. Chem.* **84**, 140–145.
Geiser, U., Gaura, R. M., Willett, R. D. & West, D. X. (1986). *Inorg. Chem.* **25**, 4203–4212.
Geiser, U., Willett, R. D., Lindbeck, M. & Emerson, K. (1986). *J. Am. Chem. Soc.* **108**, 1173–1179.
Haddad, S., Awwadi, F. & Willett, R. D. (2003). *Cryst. Growth Des.* **3**, 501–505.
Haije, W. G., Dobbelaar, J. A. L. & Maaskant, W. J. A. (1986). *Acta Cryst.* C**42**, 1485–1487.
Halvorson, K. E., Grigereit, T. & Willett, R. D. (1987). *Inorg. Chem.* **26**, 1716–1720.
Ladd, M. F. C. & Palmer, R. A. (1994). *Structure Determination by X-ray Crystallography*, 3rd ed., pp. 434–435. New York: Plenum Press.
Murray, K. & Willett, R. D. (1991). *Acta Cryst.* C**47**, 2660–2662.
Murray, K. & Willett, R. D. (1993). *Acta Cryst.* C**49**, 1739–1741.
Nonius (1998). *COLLECT*. Nonius BV, Delft, The Netherlands.
Otwinowski, Z. & Minor, W. (1997). *Methods in Enzymology*, Vol. 276, *Macromolecular Crystallography*, Part A, edited by C. W. Carter Jr & R. M. Sweet, pp. 307–326. New York: Academic Press.
Pon, G. & Willett, R. D. (1996). *Acta Cryst.* C**52**, 1122–1123.

Sheldrick, G. M. (2008). *Acta Cryst.* A**64**, 112–122.
Stucky, G. D. (1968). *Acta Cryst.* B**24**, 330–337.
Vossos, P. H., Fitzwater, D. R. & Rundle, R. E. (1963). *Acta Cryst.* **16**, 1037–1045.
Vossos, P. H., Jennings, L. D. & Rundle, R. E. (1960). *J. Chem. Phys.* **32**, 1590–1591.
Weise, S. & Willett, R. D. (1993). *Acta Cryst.* B**49**, 283–289.
Willett, R. D. (1991). *Coord. Chem. Rev.* **109**, 181–205.
Willett, R. D., Dwiggins, C. Jr, Kruh, R. F. & Rundle, R. E. (1963). *J. Chem. Phys.* **38**, 2429–2436.
Willett, R. D. & Geiser, U. (1986). *Inorg. Chem.* **25**, 4558–4561.
Willett, R. D. & Rundle, R. E. (1964). *J. Chem. Phys.* **40**, 838–847.
Zhou, P., Drumheller, J. E., Rubenacker, G. V., Bond, M. R. & Willett, R. D. (1988). *J. Phys. (Paris) Colloq.* **49**, 1471–1472.
Zordan, F., Espallargas, G. M. & Brammer, L. (2006). *CrystEngComm*, **8**, 425–431.